Pragyan Mohanty*, Dilip Kumar Mishra, Shikha Varma, Kampal Mishra and Payodhar Padhi

Influence of ultrasonic cavitation on microstructure and mechanical response of an aluminum/alumina nanocomposite

Abstract: Nanocomposites of Al and Al_2O_3 were synthesized by an ultrasonic full cavitation technique which is a novel route for synthesis of uniformly distributed nanoparticles in metal matrix composites. The transmission electron micrograph indicates the uniform arrangement of nanoparticles throughout the metal matrix and the average size of the nanoparticles are in the order of 5 nm. The selected area electron diffraction analysis shows the presence of both Al and Al_2O_3 phases, which is also evidenced from the X-ray photoelectron spectroscopy analysis. The significant improvement in hardness and Young's modulus due to the addition of a low weight fraction of nano-sized Al_2O_3 in aluminium infers that alumina nanoparticulates are distributed uniformly throughout the aluminium metal matrix. Hence, this paper shows a new method for inexpensive fabrication of bulk light weight metal matrix nanocomposites (MMNCs) by the use of non-contact full cavitation method.

Keywords: hardness; nanocomposite; TEM; ultrasonic; XPS; Young's modulus.

DOI 10.1515/secm-2014-0242
Received July 25, 2014; accepted October 23, 2014; previously published online January 20, 2015

***Corresponding author: Pragyan Mohanty,** Institute of Technical Education and Research, Department of Physics, Siksha 'O' Anusandhan University, Khandagiri Square, Bhubaneswar 751030, Odisha, India, e-mail: pragyanmohanty@soauniversity.ac.in
Dilip Kumar Mishra: Institute of Technical Education and Research, Department of Physics, Siksha 'O' Anusandhan University, Khandagiri Square, Bhubaneswar 751030, Odisha, India; and Department of Physics, College of Science, Engineering and Technology, University of South Africa, Johannesburg 1710, South Africa
Shikha Varma: Institute of Physics, Sachivalaya Marg, Bhubaneswar 751004, India
Kampal Mishra: Institute of Technical Education and Research, Department of Physics, Siksha 'O' Anusandhan University, Khandagiri Square, Bhubaneswar 751030, Odisha, India
Payodhar Padhi: Department of Mechanical Engineering, KIST, Bhubaneswar, India

1 Introduction

Metal matrix nanocomposites (MMNCs) have been attracted a lot of attention among the researchers for their numerous applications in automobile, aerospace and military industries [1–15] due to their significant mechanical properties like high specific strength, long fatigue life and improved thermal stability [16]. Several fabrication methods like mechanical alloying with high energy ball milling, nanosintering, vortex process, spray deposition, electrical plating, sol-gel synthesis, laser deposition etc. have been adopted for the synthesis of nanocomposites [3, 5, 7, 14]. The mixing of nano-sized particles is a time taking, energy consuming, and expensive in mechanical alloying technique. However, synthesis of composite by a liquid phase process is very attractive, as it can produce light-weight nanocomposite with uniform dispersion of ceramic nanoparticles [16, 17]. The uniform dispersion of nanoparticulate is necessary to enhance the elastic modulus, hardness, and tensile strength of the engineering components. Especially, the use of nanocomposite bears measure importance in automobile and aerospace industries for the fabrication of low density and high mechanical strength equipment, which can save fuel costs [18–21]. This is the reason for which aluminium is chosen as the major industrial component. Aluminum alloys, though, possess low density, but they are lacking high strength like steel and titanium alloys. Hence, an attempt has been taken to form nanocomposites of Al by a solid-state processing route or powder technology route [22–32] to enhance the mechanical strength. However, to form fully bulk-sized engineering components [23] by the uniform dispersion of nanoparticulates in the metal matrix is a challenge in the powder technology route. It is known that uniform dispersion of fine ceramic particles in the metal matrices increase the strength and wear resistance of the materials [25]. However, it is almost difficult to find the uniform dispersion of particles in solidification route due to the difference between the interaction of liquid and solid particles [27]. In this view, ultrasonic casting [28–30] is a suitable technique to forbid the agglomeration of nanoparticles in the metal matrix and to distribute nano-sized

particulates uniformly in molten melt to enhance the mechanical behaviour of the nanocomposite. High yield strength in cast Al-7wt% Si alloys by reinforcing with 2wt% nano-sized (30 nm) SiC particles has been observed by Yang and Li [29] with the advantage of the density close to pure Al. Hence, the noncontact ultrasonic method was almost able for uniform dispersion of nanoparticulates in metal matrix to increase the strength of the composites with the same density of the pure metal.

In this study, metal matrix nanocomposites were synthesized by ultrasonic full cavitation technique by two mixing processes to avoid the agglomeration and clustering of nanoparticles. The structural and mechanical properties have been studied using various experimental tools to prove that the ultrasonic cavitation technique is a novel technique for the synthesis of metal matrix nanocomposites.

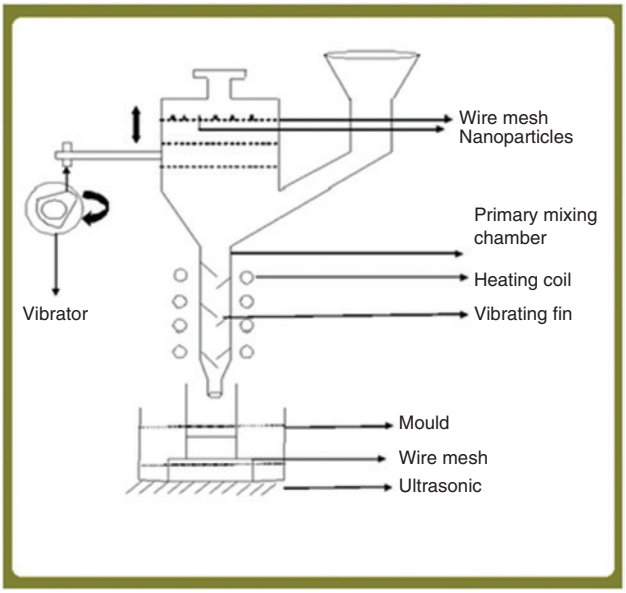

Figure 1 Schematic diagram of ultrasonic full cavitations experimental setup.

2 Materials and methods

For the production of nano-sized Al_2O_3 particulates of average size 10–12 nm, commercial available alumina powder (NALCO, Bhubaneswar, India) of micron size were ball milled for 72 h using a high energy Fritsch Pulverisette-5 planetary ball mill with WC grinding balls. The ball milling was done at 300 RPM, and the tollune was used as the reagent. Commercially available aluminium (NALCO, Bhubaneswar, India) of composition of 0.96%Fe-0.43%Mg-0.26%Si was reinforced with this nano-sized Al_2O_3 by the noncontact full cavitation method. The schematic diagram of the experimental setup, shown in Figure 1, consists of an ultrasonic generator (RK-100H, Bandelin, Germany). The mixing of nano-sized powders with aluminium melt has been performed by primary and secondary mixing process. In primary mixing, the nanoparticulates were mixed up with molten aluminium melt with the help of a vibrating motor. Aluminium was melted at a temperature of 760°C, and the melt was placed in the ultrasonic chamber. An ultrasonic chamber consists of a steel die of 60 mm length, 40 mm diameter, and 1.5 mm thickness and a primary mixing unit. Sufficient water circulation facility had been provided around the die for transmission of ultrasonic waves from all sides of the chamber. The mould was heated with an ambient temperature to avoid thermal cracking and was placed in an ultrasonic chamber under frequency of 35 KHz. Further, nearly 350 g of liquid aluminium and 1.5wt% of alumina nanoparticulates were poured into a vibrating mould. The vibration was continued for 5 min. The mould inside the ultrasonic chamber was surrounded by water for proper transmission of ultrasonic waves. Within a few minutes solid nanocomposite was formed.

The nanocomposite ingot was cylindrical in shape and cut along the transverse direction in two equal halves. Then one half of the composite was cut longitudinally into five

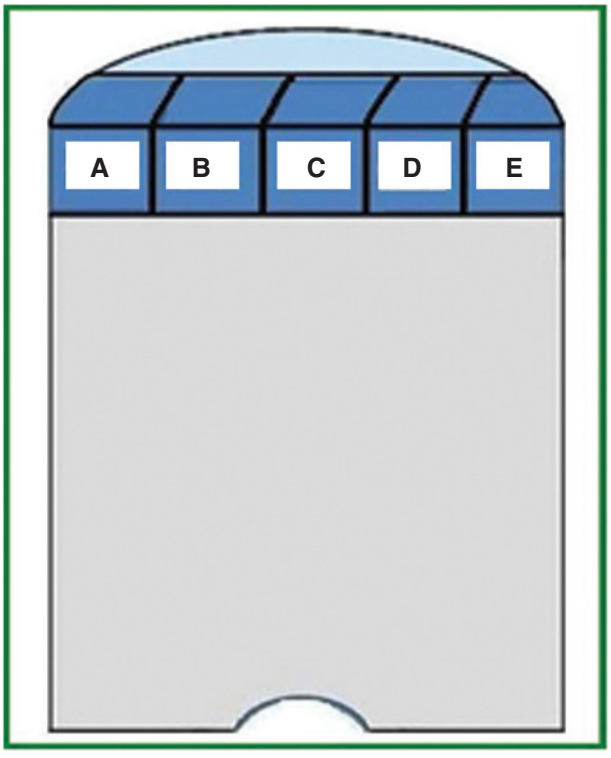

Figure 2 Cross-sectional view of the ingot.

small pieces of nearly equal size of 1 cm^2 cross-sectional area and 0.5 cm thickness (shown in Figure 2). Each of the specimens is lettered as a, b, c, d, and e, respectively, from left to right. Then each sample surface was ground and polished with submicron-sized emery paper of number 100 and 200 grits. These grounded and polished specimens were considered for the characterization to have a physical and mechanical feature of the nanocomposites. To study the distribution of nanoparticles in the Al matrix and the microstructure, transmission electron microscopy characterization (JEOL JEM 2100) has been carried out including the selected area electron diffraction analysis. X-ray photoelectron spectroscopy (XPS) measurements were performed using a VG ESCA system using the Mg K_α X-ray source with pass energy of 20 eV at a base pressure of 1.0×10^{-10} Torr. To have a detailed idea about hardness and Young's modulus, nanoindentation tests were performed with respect to penetration depth for each of the specimens using a UMIS nanoindentation system (Fischer Cripps, Forestville, Sydney, Australia). The load versus penetration depth, hardness versus penetration depth, and Young's modulus versus distance have been measured for each location of the sample one by one with the help of nanoprobe indentation using a diamond Bekovich indenter. The maximum load of the nanoprobe indentation was restricted to 20 mN. The mathematical expression used for the determination of hardness and Young's modulus using a nanoindenter has been described in literature [33, 34].

3 Results and discussion

Figure 3A shows the transmission electron micrograph of Al and Al_2O_3 composites. The micrograph shows the uniform distribution of nanocomposites of Al_2O_3 throughout the Al matrix. The white coloured spot represents the nanoparticles of Al_2O_3, whereas the black coloured surface represents the Al matrix. The average size of alumina nanoparticles is within the range of 5 nm. Even the size of the nanopowders of alumina is taken in the order of 10–12 nm in the Al matrix, but during mixing, there is a possibility of fragmentation of nanoparticles due to ultrasonication, which gives rise to the decrease in particle size of the composite.

Similar types of micrographs have been observed throughout the matrix with a slight variation of particle size. This confirms that the ultrasonic cavitations technique is a good mixing technique for the formation of nanocomposites of Al and Al_2O_3 compared to the conventional technique. To confirm the presence of Al and Al_2O_3, a selected area electron diffraction (SAED) pattern has been shown in Figure 3B.

The SAED pattern always provides information about the crystallographic idea of Al and Al_2O_3. The pattern clearly establishes the long-range ordering of Al and Al_2O_3 matrix in a particular crystallographic orientation. The crystallographic plane of the nanocomposite Al_2O_3 is very difficult to be established from X-ray diffraction analysis in consideration of the Al. The maximum interplanar spacing between two atomic planes is on the order of 2.337 Å in Al [35], whereas the same interplanar spacing in Al_2O_3 is on the order of 2.551 Å [36]. Hence, X-ray diffraction pattern is unable to establish the presence of Al and Al_2O_3 within the resolution of X-ray. However, the selected area electron diffraction pattern is a novel tool to distinguish the presence of Al and Al_2O_3 that has been clearly reflected in Figure 3B with the crystallographic planes. The crystallographic planes representing Al_2O_3 are

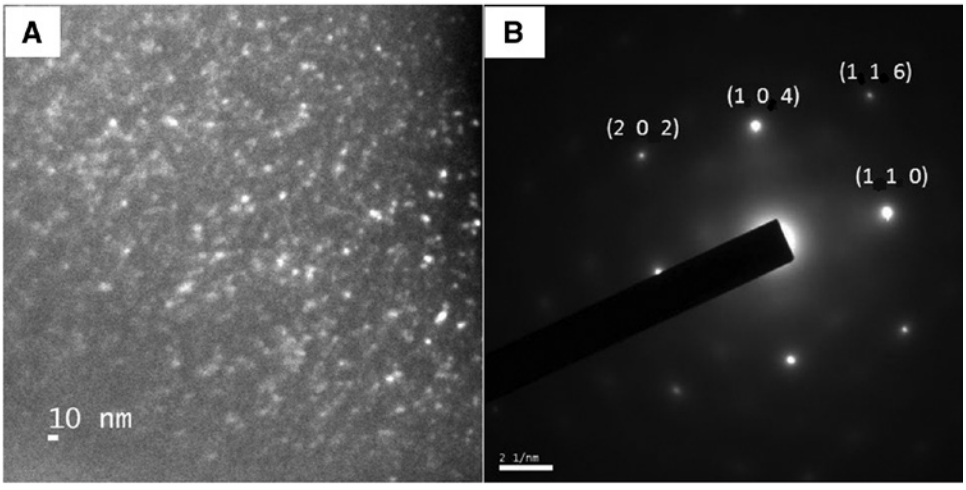

Figure 3 (A) TEM picture and (B) selected area electron diffraction patterns of Al and Al_2O_3 nanocomposites.

indexed in the SAED pattern. The TEM picture and SAED patterns reflect the uniform distribution of nanopowders of Al_2O_3 in Al matrix, which may enhance the mechanical performance of the composites.

The survey spectrum with the individual spectrum of C, O, and Al are shown in Figure 4. The survey spectrum (Figure 4A) reveals the presence of Al and O including a high intensified peak of C1s. The signature of the C1s comes from the environment and from the sample holder in which carbon tape is used to stick the sample. The C1s peak is taken as a standardised binding energy to analyse other elements present in the sample. The C1s spectrum is shown in Figure 4B. The binding energy at 284.6 eV attributes to free carbon [37], which means that the signature of C found in the composite is not a contaminant of the nanocomposites.

The X-ray photoelectron spectra for Al2p and O1s are shown in Figure 4C and D. The maximum intensity of the O1s peak is centred at 531.1 eV (Figure 4C). This binding energy is attributed to the bonding of Al with O. It infers that alumina is present in the sample with Al matrix. However, the presence of Al matrix is established from core level spectrum of Al. The core level spectrum of Al2p is shown in Figure 4D. The characteristic curve is deconvoluted into three peaks. The lower binding energy and medium binding energy at 70 eV and 72.9 eV are attributed to the Al, whereas higher binding energy at 74.6 eV is attributed to the bonding of Al and O [37]. This infers that both Al and Al_2O_3 are present in the nanocomposites.

The load versus penetration depth is shown in Figure 5 for the entire specimen specified in Figure 2 for Al and Al_2O_3 nanocomposites. The maximum load of 20 mN is applied in all specimens with a variation of 1 mN for each set of measurements having a drift rate of 0.06 nm/s. With the increase of load, penetration depth increases. Figure 5A–E shows that in first cycle of applied load for a maximum load of 20 mN, the penetration depths are 0.55 μm, 0.52 μm, 0.57 μm, 0.58 μm and 0.54 μm, respectively. For the same maximum load of 20 mN, the penetration depth varies in a range of ±0.03 μm. It is observed that

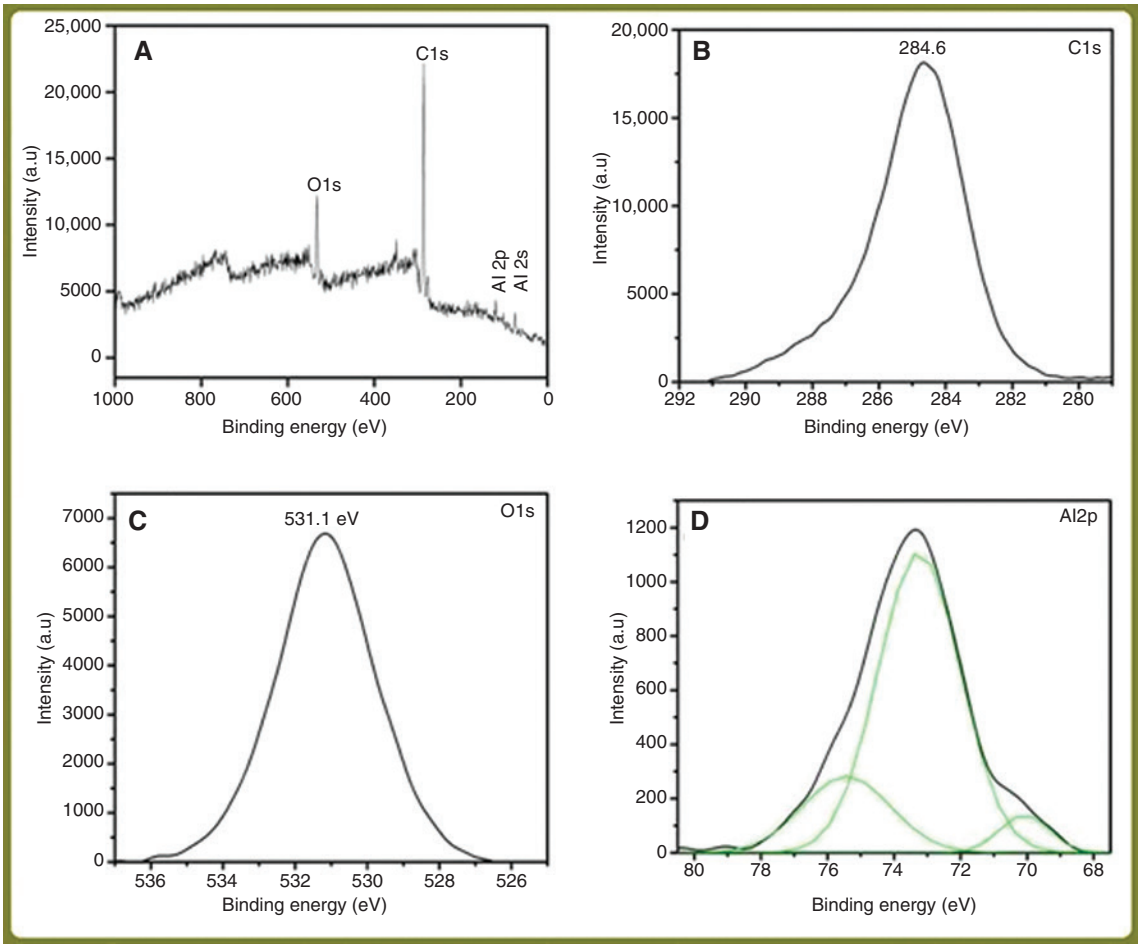

Figure 4 X-ray photoelectron (A) survey spectrum, (B) C1s core level, (C) O1s core level, and (D) Al2p core level X-ray photoelectron spectrum of Al and Al_2O_3 nanocomposites.

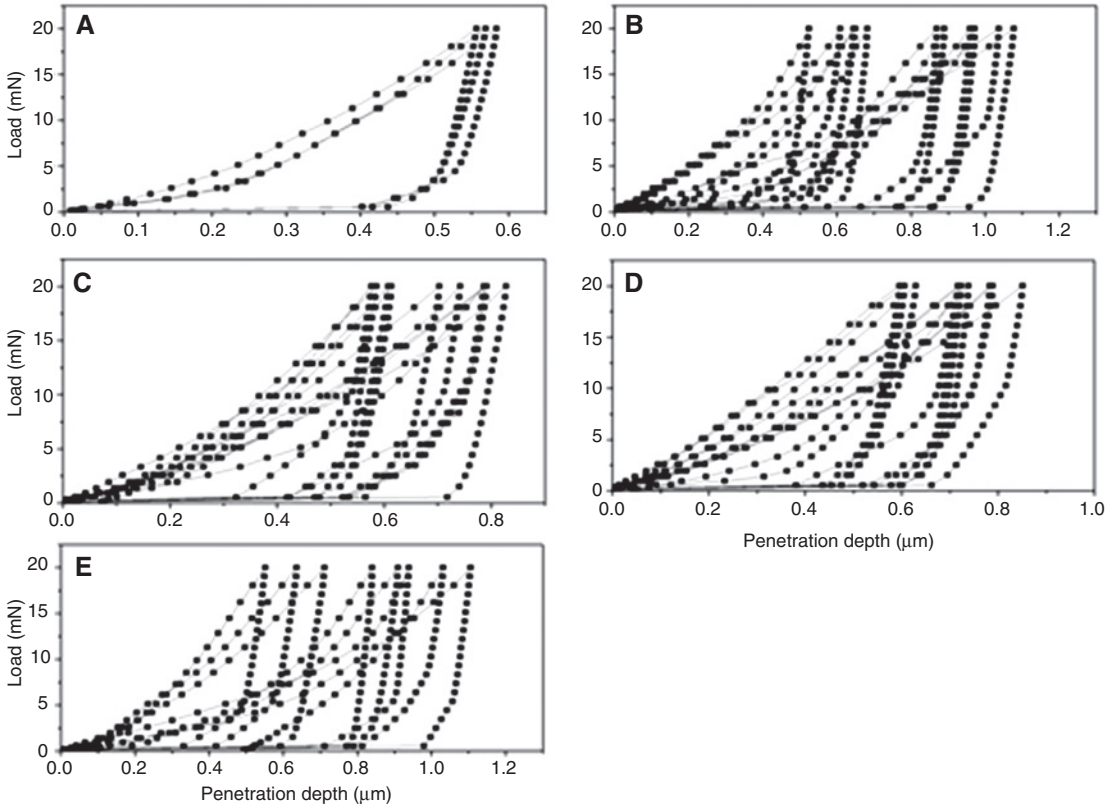

Figure 5 Load vs. penetration depth of Al and Al_2O_3 nanocomposites for all five specimens taken from the half of the cylindrical cross section.

at the periphery regions (Figure 5A and E), the penetration depths are almost constant, whereas in the middle regions, the penetration depth is slightly more. This is because of the distribution of more nanoparticles or presence of more agglomerates in periphery region in comparison to the middle portion. It occurs due to the action of centrifugal force on nanoparticles during the mixing of matrix and nanopowders. So nearer the periphery region, the depth of indentation is less in comparison to the middle region of the bulk composite. For the first cycle of the measurement, it is observed that the penetration depth is almost equal (0.55±0.03 μm). That means that distribution of nanoalumina powder is uniform throughout the matrix for which the penetration depth does not alter, which may enhance the hardness and elasticity modulus. The study infers that nanoparticulates are mostly having even distribution throughout the aluminium metal matrix, which is evidenced from the TEM picture.

Figure 6 shows the hardness versus penetration depth of Al and Al_2O_3 nanocomposites for five specimens. The monotonic variation of hardness is observed as the penetration depth increases with the application of load pertaining to the same line profile for all five locations of the sample. It is observed in Figure 6 that when penetration depth is small, hardness is more. As penetration depth increases, hardness gradually decreases. It is observed that for a constant penetration depth of each of the location, the hardness value is almost the same. For all five

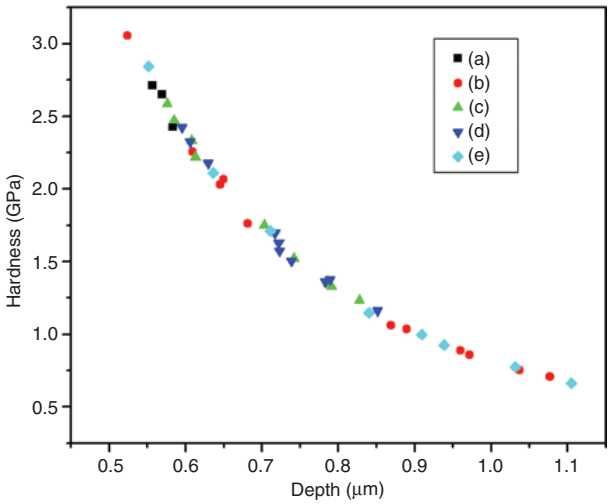

Figure 6 Hardness vs. penetration depth of Al and Al_2O_3 nanocomposites for all five specimens taken from the half of the cylindrical cross section.

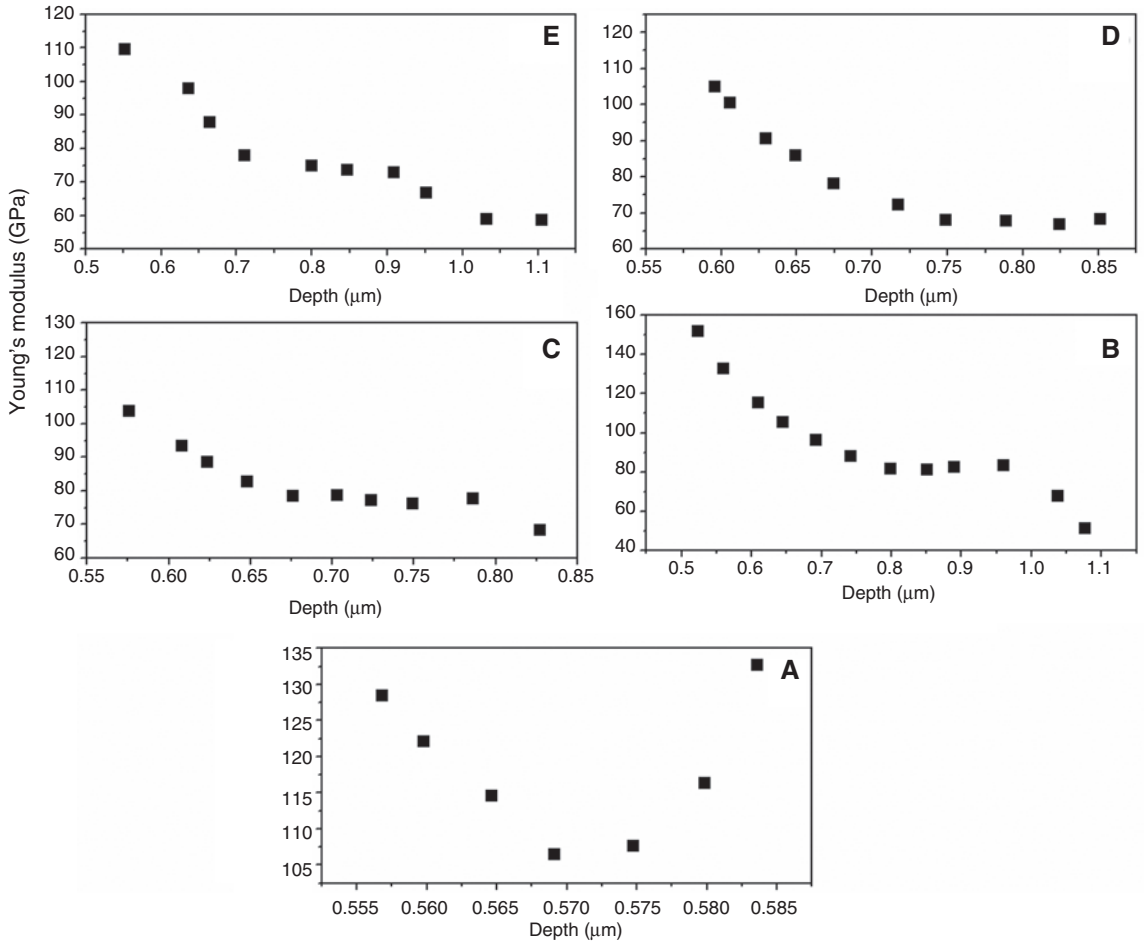

Figure 7 Young's modulus vs. penetration depth of Al and Al_2O_3 nanocomposites for all five specimens taken from the half of the cylindrical cross section.

samples from different locations hardness is almost the same, which signifies the uniform distribution of nanoparticles in the aluminium matrix. This gives isotropic mechanical properties of the composites.

Figure 7A–E shows the plots between Young's modulus versus penetration depth for all the locations of the sample. These figures show that when the penetration depth is less, Young's modulus is more. The elastic property is more in a nanoparticle system compared to the bulk sample. As penetration depth increases, Young's modulus gradually decreases due to clustering of nanoparticles in some locations. In periphery regions (Figure 7A and E), for a depth of 0.55 μm, the difference of elasticity value is not significant. That means for a particular depth of applied load, values of Young's modulus are almost the same for each location. This also ensures that nanoparticulates have almost even distribution throughout the metal matrix. The load, hardness, and Young's modulus versus penetration depth establish a fact that the ultrasonic full cavitation technique is the most suitable technique for the preparation of nanocomposites with uniform distribution of nanoparticles throughout the matrix. In addition, the restriction of agglomeration of the nanoparticles in the matrix is another advantage to enhance the physical and mechanical behaviour of the metal matrix nanocomposites.

4 Conclusions

Following conclusions have been made from our experimental observations:

1. Noncontact full cavitation technique is a novel route for synthesis of nanocomposites.
2. TEM analysis indicates the uniform arrangement of nanoparticles through the metal matrix, and the average size of the nanoparticles is on the order of 5 nm. The SAED analysis shows the presence of both Al and Al_2O_3.

3. The hardness and Young's modulus results infer that alumina nanoparticulates are distributed uniformly over the aluminium metal matrix.
4. This uniform distribution will increase the strength, light weight, and hardness of the nanocomposite more than the metal matrix and micrometric composite.

Acknowledgments: Mr. Santosh Choudhary, IOP, Bhubaneswar is gratefully acknowledged for his assistance in recording the XPS data. Author D.K. Mishra is thankful to UNISA for providing the position of Visiting Researcher under the visiting researcher support programme.

References

[1] Huang ST, Zhou L, Chen J, Xu LF. *Mater. Manuf. Proc.* 2012, 27, 1090–1094.
[2] Morita M. *Adv. Compos. Mater.* 2011, 4, 237–246.
[3] Eskandari A, Aminzare M, Razavi hesabi Z, Aboutalebi SH, Sadrnezhaad SK. *Ceram. Int.* 2012, 38, 2627–2632.
[4] Dong G, Zhang H, Zhou M, Zhang Y. *Mater. Manuf. Proc.* 2013, 28, 999–1002.
[5] Ni X, Li J. *J. Alloys Compd.* 2013, 558, 62–67.
[6] Thomson KE, Jiang D, Yao W, Ritchie RO, Mukherjee AK. *Acta Mater.* 2012, 60, 622–632.
[7] Aminzare M, Mazaheri M, Golestani-fard F, Rezaie HR, Ajeian R. *Ceram. Int.* 2011, 37, 9–14.
[8] Sarkar S, Das PK. *Mater. Chem. Phys.* 2012, 137, 511–518.
[9] Chen LY, Weiss D, Morrow J, Xu JQ, Li XC. *Manuf. Lett.* 2013, 1, 62–65.
[10] Poirier D, Drew RAL, Trudeau ML, Gauvin R. *Mater. Sci. Eng.: A* 2010, 527, 7605–7614.
[11] Shehata F, Fathy A, Abdelhameed M, Moustafa SF. *J. Alloys Compd.* 2009, 476, 300–305.
[12] Ibrahim A, Moamed FA, Lavernia EJ. *J. Mater. Sci.* 1991, 26, 1137–1156.
[13] Gudlur P, Muliana A, Radovic M. *Composites Part B: Eng.* 2014, 58, 534–543.
[14] Nowak S, Ochin P, Champion Y. *Mater. Manuf. Proc.* 2009, 24, 1162–1167.
[15] Mussert KM, Vellinga WP, Bakker A, Van Der Zwaag SA. *J. Mater. Sci.* 2002, 37, 789–794.
[16] Arranz-Andrés J, Pulido-González N, Fonseca C, Pérez E, Cerrada ML. *Mater. Chem. Phys.* 2013, 142, 469–478.
[17] Akio K, Atsushi O, Toshiro K, Hiroyuki T. *J. Jpn. Inst. Metals* 1999, 49, 149–154.
[18] Suryanarayana C, Ivanov E, Boldyrev VV. *Mater. Sci. Eng.: A* 2001, 151, 304–306.
[19] Kiminami CS, Basim ND, Kaufman MJ, Amateur MF, Eden TJ, Galbraith GJ. *Key Eng. Mater.* 2001, 189–191, 503–508.
[20] Huda MD, Hashmi MSJ, EI-Baradie MA. *Key Eng. Mater.* 1995, 104–107, 37–64.
[21] Ejiofor JU, Reddy RG. *J. Mater.* 1997, 49, 31–37.
[22] Simoes S, Viana F, Reis MAL, Vieira MF. *Compos. Struct.* 2014, 108, 992–1000.
[23] Inoue A. *Progr. Mater. Sci.* 1998, 43, 365–520.
[24] Koch CC. *Nanostruct. Mater.* 1997, 9, 13–22.
[25] Lu K. *Mater. Sci. Eng. R* 1996, 16, 161–221.
[26] Das D, Chatterjee PP, Manna I, Pabi SK. *Scr. Mater.* 1999, 41, 861–866.
[27] Datta MK, Pabi SK, Murtty BS. *Appl. Phys.* 2000, 87, 8393–8400.
[28] Inoue A. *Materials Science Foundation 4*, Trans. Tech. Netherlands, 1998, pp. 1–116.
[29] Yang Y, Li X. *J. Manuf. Sci. Eng.* 2007, 129, 252–255.
[30] Haghayeghi R, Kapranos P. *Mater. Lett.* 2013, 105, 213–215.
[31] Benameur T, Innoue A, Masumoto T. *Nanostruct. Mater.* 1994, 4, 303–322.
[32] Ecert J. In *Properties and Potential Applications*, Koch CC, Ed., Noyes, New York, 2002, pp 423–525.
[33] Oliver WC, Pharr GM. *J. Mater. Res.* 1992, 7, 1564–1583.
[34] Behera D, Mishra DK, Pradhan SK, Sakthivel R, Mohanty S. *Appl. Surf. Sci.* 2011, 258, 1103–1108.
[35] Swanson HE, Tatge E. *Natl. Bur. Stand. (U.S.), Circ., 539*, 1953, 1, 21.
[36] Liu RS, Shi WC, Cheng YC, Huang CY. *Mod. Phys. Lett.* 1997, 11, 1169.
[37] Wagner CD, Riggs WM, Davis LE, Moulder JF, Muilenberg GE. *Handbook of X-ray Photoelectron Spectroscopy*, Perkinelmer Corp., Waltham, MA, 1979.